Brandon R. Travis
Ph.D.*

Thomas D. Christensen
M.D.

Morten Smerup
M.D.

Morten S. Olsen
M.S.

J. Michael Hasenkam
M.D., D.M.Sc.

Department of Cardiothoracic and Vascular Surgery,
Århus University Hospital, Skejby Sygehus,
Århus, Denmark
Institute for Experimental Clinical Research,
Århus University Hospital, Skejby Sygehus,
Århus, Denmark

Hans Nygaard
M.S., D.M.Sc.
Department of Cardiothoracic and Vascular Surgery,
Århus University Hospital, Skejby Sygehus,
Århus, Denmark
The Engineering College of Århus,
Århus, Denmark

An In Vivo Method for Measuring Turbulence in Mechanical Prosthesis Leakage Jets

This work introduces a method for the in vivo measurement and analysis of turbulence within the leakage of a mechanical heart valve. Several analysis techniques were applied to ultrasound measurements acquired within the atrium of a pig, and error associated with these techniques was analyzed. The technique chosen applies cyclic averaging to mean and maximum velocity measurements within small, normalized phase windows to calculate Reynolds normal stresses in the direction of the ultrasound beam. Maximum shear stresses are estimated from these normal stresses using an analytical technique. The stresses observed were smaller than those reported from previous in vitro simulations. [DOI: 10.1115/1.1644563]

Introduction

When the function of one of the valves of the heart becomes severely compromised, it is often necessary to replace the faulty valve with a functional prosthesis. The choice of a mechanical valve provides the patient with a durable replacement with good hemodynamics. However, mechanical prostheses promote thromboembolism, and patients with these valves must undergo lifelong oral anticoagulation therapy.

The design characteristics of mechanical prostheses that promote thrombosis are currently unknown. However, recent clinical experience and subsequent in vitro analysis of the Medtronic Parallel (MP) prosthesis suggests that leakage flow is a potential culprit. Although this valve design offered an improvement in forward flow hemodynamics [1], it performed poorly in clinical trials; approximately 20% of patients in these trials developed thrombosis [2]. Explants from these patients showed that thrombus formation was localized to the pivot areas [3] (Fig. 1). Flow through the pivots of bileaflet prostheses had not been previously investigated, and novel in vitro experiments using a valve with a clear housing were performed to study this flow. Analysis of data from these experiments revealed regions of highly disturbed vortical flow within the gaps of the MP pivots during the phase of the cardiac cycle when the valve was closed, the leakage phase [3,4]. Turbulent shear stresses as high as 360 N/m^2 were reported in these areas [4]. Furthermore, the length scale of the smallest turbulent eddies was found to be the same order of magnitude as the diameter of blood cells [4], suggesting that leakage through valve pivots can disrupt the blood elements and initiate thrombosis. The leakage flow patterns of many prosthetic valve designs have been investigated in vitro [5–12], and other in vitro experiments have demonstrated the tendency of leakage to induce damage to the cells of the blood [13–15].

While impressive in what they have shown thus far, in vitro simulations may not closely approximate the flow patterns and turbulence of mechanical prosthesis leakage flow. Previous turbulence studies of leakage flow have been carried out in rigid simulators, using fluids that mimic the viscosity of blood at high shear rates. The rigid simulators used in the studies of leakage flow through prosthetic heart valves do not closely simulate the natural geometry of the circulation. Although often analyzed as free turbulent jets, which are independent of chamber geometry, the leakage of prosthetic heart valves may impinge on the walls of the heart, and definitely have interaction with incoming forward flow. In addition, previous turbulence studies on leakage flow through prosthetic valves have used Newtonian blood analog fluids. The length scales of the leakage gaps are only one order of magnitude larger than the length scales of the blood cells themselves, which may cause blood to behave in a non-Newtonian fashion. Many studies on capillary flow and a study on leakage flow through prosthetic valves suggest that blood does not behave in a Newtonian fashion during the leakage phase [16,17]. Since these possible shortcomings could have a large effect on the magnitudes of leakage jet turbulence, it may be necessary to study this turbulence in vivo, using whole blood and a physiologic cardiac geometry. The purposes of this work were to introduce such a technique for the measurement of leakage jet turbulence, to develop a data analysis

*Corresponding author: Research Fellow, Department of Cardiothoracic and Vascular Surgery, Århus Universitetshospital, Skejby Sygehus, Brendstrupgaardsvej, 8200 Århus N, Denmark. Phone: +45 89495485; Fax: +45 89496016; e-mail: brandontravis2001@yahoo.com

Contributed by the Bioengineering Division for publication in the JOURNAL OF BIOMECHANICAL ENGINEERING. Manuscript received by the Bioengineering Division September 5, 2002; revision received October 1, 2003. Associate Editor: C. R. Ethier.

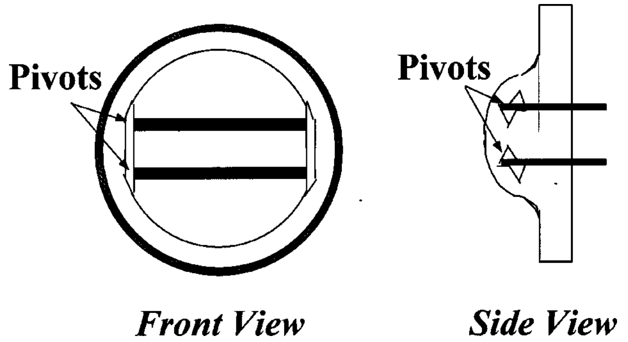

Fig. 1 A bileaflet mechanical prosthesis, emphasizing the pivot region.

method for measurements collected using this technique, and to compare magnitudes of Reynolds stress observed from this method and simulations previously performed in vitro.

Materials and Methods

Experimental Setup. This experiment was performed using a 90 kg female pig, of mixed Landrace and Yorkshire breed. This in vivo model was chosen because the pig heart resembles that of a human in geometry and size. Upon arrival to the laboratory, the pig was intramuscularly anesthised with 50 mg midazolam (Dormicum®) and 5 mg azapevon (Stresnil®). When the pig was still and relaxed, intravenous access was obtained through an ear vein. Through this port, the pig received an additional injection of 50 mg midazolam and 1000 mg ketamin (Ketalar®) to enable endotracheal intubation. This tubing was coupled to a ventilator, and anesthesia maintained with midazolam (25 mg/kg/hr), ketamin (1250 mg/kg/hr), and fentanyl (Haldid®, 1000 μg/kg/hr) throughout the experiment. Pancouronium (Pavulon®, 10 mg/kg/hr) was used as muscle relaxant. ECG and venous and arterial blood pressure were continuously monitored during the experiment using fluid filled catheters connected with a CardioMed (Model 4008, CardioMed A/S, Oslo, NO). These pressure measurements were obtained via the surgically exposed right external jugular vein and right carotid artery.

A midline sternotomy was performed to expose the heart. After full heparinization, venous and aortic cannulae were introduced. Cardiopulmonary bypass was then started to allow aortic cross-clamping and cold cardioplegic arrest. This arrest was performed by the infusion of St. Thomas' solution in the aortic root every 20 min. Blood gasses and hemodilution were measured every 20 min during bypass using an ABL (Radiometer, Copenhagen, DK, Model 615). The mitral annulus was exposed using a left atrial incision. A St. Jude Medical standard size 29 mitral valve was mounted and sewn tightly to a traverse apparatus using 15 2-0 pledgeted mattress sutures with the pledgets on the atrial side. This traverse apparatus (Fig. 2), enabled an ultrasound transducer to be moved in three dimensions with respect to the valve, with an accuracy of $\pm 1/8$ mm. The valve and mounting portion of the apparatus were implanted in the anti-anatomic position of the mitral annulus of the pig. The atrium was sutured around the rod connecting the mounting portion of the apparatus to the transversing portion. The traversing portion of the apparatus, which was located outside the heart after the suturing of the atrium, allowed manual movement of the ultrasound transducer during the experiment. The surgery simulated a normal mitral valve replacement, with the exception that the atrium was sewn around a stiff metal rod.

Micro-tip catheter pressure transducers (Millar Instruments Inc., Houston, TX, USA, Model SPC-350), interfaced with battery powered amplifiers, were inserted into both the left atrium and left ventricle. Cardiopulmonary bypass was terminated, and the heart

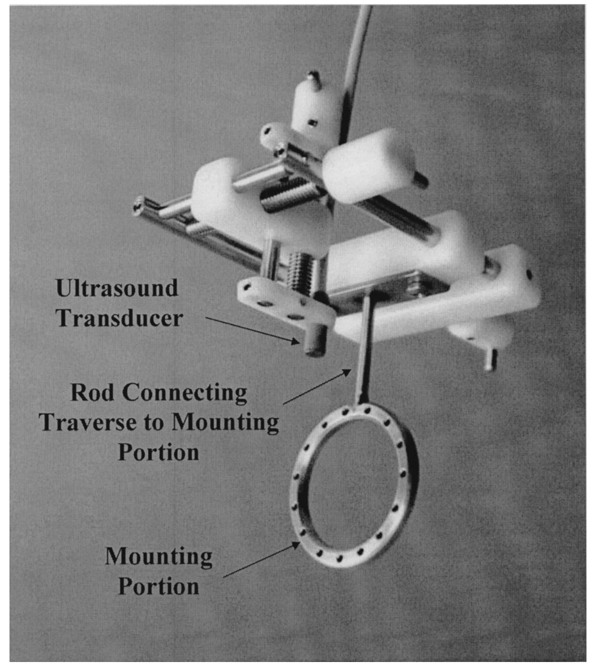

Fig. 2 Traverse apparatus used to move ultrasound transducer. The mounting portion of the apparatus is sewn to the valve, allowing a precise positioning of an ultrasound transducer with respect to the valve.

was allowed to resume sinus rhythm. A custom 10 MHz ultrasound transducer was placed on the traversing portion of the apparatus. This transducer was connected to a VingMed amplifier (Vingmed, Horten, Norway, Model ALFRED), which was operated in the pulsed mode and modified to allow the measurement of turbulent velocity fluctuations. The amplifier quantified velocities from the Doppler signal by a zero-crossing algorithm. Previous tests on the PDU system [18] have quantified the -3 dB cutoff frequency of the ultrasound system at 200 Hz. The sample volume for this apparatus was a cylinder approximately 1.5 mm in diameter and 1.0 mm in length. The pulse repetition frequency of the transducer/amplifier pair varied between 29 and 42 kHz during the experiment, depending on the depth of measurement. The VingMed and Millar amplifiers were interfaced with a PCM data recorder (TEAC, Tokyo, Japan, Model RD 180T) and an analog/digital converter (National Instruments, Austin, TX, USA, Model AT-MIO16-E2). Digital information from the converter was interpreted using a computer. Peak pressure within the left ventricle of the pig was measured between 91 and 130 mm Hg throughout data acquisition.

After the necessary measurements were acquired, the pig was euthanized by direct injection of a saturated potassium chloride solution into the left ventricle. All procedures were conducted according to approval from the Danish Inspectorate of Animal Experimentation.

Data Acquisition. Before measurements were obtained, the locations of the leakage jets had to be determined. Approximate locations of leakage jets with respect to several bileaflet valves have been determined earlier in a series of experiments by Steegers et al. [9]. The results of these experiments were used to define an interrogation area 1 mm upstream of the pivot guards of the valve (approximately 5 mm upstream of the pivots), within which half of the leakage jets of the valve should be located (Figure 3). The traversing apparatus was adjusted until the ultrasound transducer contacted the atrial wall, and was positioned 1 mm proximal to the pivot guards of the valve housing. The traversing apparatus was used to move the ultrasound transducer in 1

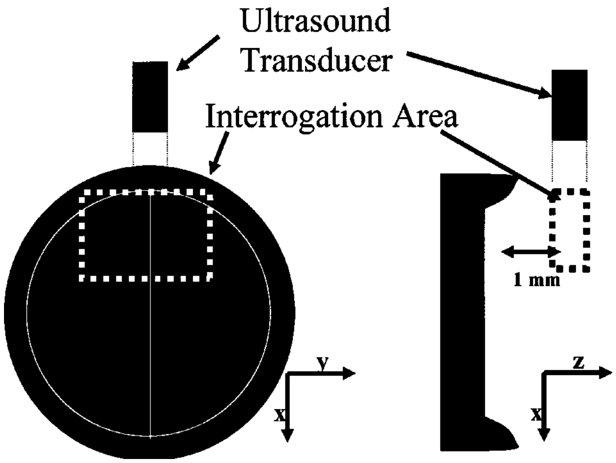

Fig. 3 Interrogation area of study with respect to the valve and ultrasound transducer. The Cartesian axes used in this study are defined here.

mm increments over the interrogation area, which corresponded to depths between 15 and 26 mm. After each movement, a custom program based on LabView software (National Instruments, Austin, TX, USA, Version 6.0i) was used to acquire velocity data during the leakage phase of one cardiac cycle. Acquisition of data was triggered by the rise in left ventricular pressure during the beginning of systole. A 10 Hz high pass filter (fifth order Butterworth) was imposed on the collected data, and the filtered data were used to calculate a first order estimate of Reynolds normal stress from mean velocity measurements of the ultrasound transducer. This estimate was written down on a map of the interrogation area. Large maxima within the interrogation area represented the locations of the leakage jets, and were used to define the measurement area.

Each measurement area consisted of a square area drawn around one of the maxima. The square was parallel with the plane of the valve housing, 1 mm proximal to the pivot guards of the valve, and had sides of 6 mm. The measurement area was traversed in 0.5 mm increments. The aforementioned turbulent stress estimation program was run after each movement in this area. If the value of Reynolds normal stress returned by the estimation program was greater than 2/3 the maximum, the measurement location was noted, and twenty cycles of velocity and pressure measurements were acquired by the data recorder. Both mean and maximum velocity signals from the VingMed amplifier were measured. Mean velocity signals were determined by averaging the range of Doppler shifts registered by the transducer after a single Doppler pulse. Maximum velocity signals were determined from the maximum in Doppler shift registered by the transducer after a single Doppler pulse. Therefore, the mean velocity signal represents the mean velocity of all blood cells within the sample volume at a particular time, while the maximum velocity signal represents the velocity of the single or small number of blood cells moving at the highest velocity within the sample volume at a particular time. Left ventricular pressure, left atrial pressure, mean velocity, and maximum velocity measurements were digitized and acquired by the recorder at a sampling rate of 5 kHz.

Experiments were attempted at a proximal distance of 5 mm from the valve as well, but could not be collected because the atrial wall blocked flow at this location.

Data Analysis. The leakage portion of each cycle of data obtained by the recorder was transferred to a computer via the analog/digital converter mentioned previously. Acquisition of this data by the computer was triggered by a rise in ventricular pressure above 30 mm Hg, and acquisition was stopped when the pressure dropped below 30 mm Hg. The systolic duration, defined in this study as the amount of time the ventricular pressure was greater than 30 mm Hg within a given beat, varied between 340 and 391 ms during the course of the experiment. The maximum difference in systolic duration between beats acquired at the same measurement location was 26 ms.

The acquired data were analyzed visually using another LabView based program. If no velocity signal was present during a cycle, or if the left ventricular pressure signal during this cycle were markedly different from that of other cycles at the same measurement location, data from this cycle were removed from the analysis. Due to the differences in systolic duration within the experiment, placement of the remaining data with respect to time was normalized by systolic time duration. Mean and maximum velocity data in the remaining cycles were divided into discreet phase windows for analysis. Two phase window sizes were used in these studies, a longer window (window L) and a shorter window (window S). These windows were overlapped by 50% of their time duration. The number of the windows composing the systolic period was held constant at 17 for window size L and 41 for window size S. The time lengths of the windows were equivalent within a given beat, but varied between beats in window length and number of measurements within each window. The maximal window lengths were 49 and 20 ms, respectively, and the minimum number of measurements within each window were 4263 and 1705.

Average velocities (u_{oo}) within each of the phase windows were calculated by ensemble averaging of the maximum velocity measurements (u_{ij}):

$$(u_{oo})_x = \frac{\sum_{l=1}^{a} \sum_{m=1}^{n} (u_{lm})_x}{N} \tag{1}$$

where a represents the number of cycles, n the number of measurements associated with a particular phase window of the ath cycle, and N the total number of measurements in this phase window. These average velocity values represent only the velocity component in the direction of the ultrasound beam. To estimate peak velocity magnitudes in the jets, these average velocities were corrected for direction:

$$u_{\text{peak}} = \frac{(u_{oo})_x}{\cos \theta_x} \tag{2}$$

where θ_x is the angle between the x axis, defined in Fig. 3, and the axis of the leakage jet. Values of θ_x are documented in Table 1, and were estimated from previous studies of the leakage jet axis with respect to the valve [9,11]. It should be noted that the axes of the leakage jets did not lie on the same axis as the forward flow across the valve.

Turbulent normal stresses were calculated from both the mean and the maximum velocity measurements using three analysis techniques. In the first of these techniques, ensemble averaging, turbulent normal stresses were calculated using the variation in velocity measurements as follows:

$$\sigma_{x,PDU} = \frac{\sum_{l=1}^{a} \sum_{m=1}^{n} \rho((u_{lm})_x - (u_{oo})_x)^2}{N} \tag{3}$$

where ρ is the density of the blood, taken as 1.06 g/cm^3. The ensemble averaging technique has been the most widely used analysis technique in current literature.

The second analysis technique, cyclic averaging, recognizes that cyclic variation can introduce error into the calculations of turbulent stresses from velocity measurements. This technique statistically decomposes the total velocity variation into two components:

$$\sum_{l=1}^{a}\sum_{m=1}^{n}(u_{lm}-u_{oo})^2=\sum_{l=1}^{a}n_l(u_{lo}-u_{oo})^2+\sum_{l=1}^{a}\sum_{m=1}^{n}(u_{lm}-u_{lo})^2 \tag{4}$$

where:

$$u_{lo}=\frac{\sum_{m=1}^{n}u_{lm}}{n} \tag{5}$$

represents the mean velocity within a particular phase window during the lth cycle. The first term on the right hand side of Eq. (4) represents velocity variation caused by mean velocity differences between cycles, while the second term is defined as the turbulent fluctuations. This method thus removes a source of error from calculation of the turbulent normal stresses [11]. Turbulent normal stress in a particular combination of measurement location and phase window was calculated by:

$$\sigma_{x,PDU}=\frac{\sum_{l=1}^{n}\sum_{m=1}^{n}\rho((u_{lm})_x-(u_{lo})_x)^2}{N-a} \tag{6}$$

The last analysis technique used, high pass filtering, has been used by researchers in this laboratory in the past to calculate turbulent normal stresses [19]. In this method, a 10 Hz high pass filter (5th order Butterworth) was applied to the data. This filter removed low frequency velocity fluctuations from the data, which include the underlying mean velocity waveform and any large-scale structures with a frequency lower than 10 Hz. Higher frequency velocity fluctuations, such as those due to turbulence, were present after the filtration. After application of the filter, remaining velocity data were divided into phase windows, squared, and averaged:

$$\sigma_{x,PDU}=\frac{\sum_{l=1}^{a}\sum_{m=1}^{n}\rho(u_{lm,f})_x^2}{N} \tag{7}$$

Error Estimation and Correction. Velocity measurements from Doppler ultrasound are contaminated with variance resulting from phase differences in the returning sound signal and velocity gradients across the sample volume [20]. This contamination should be removed after calculation of the turbulent stresses. Ambiguity resulting from phase differences in the returning sound signal can come from two independent sources. One of these sources is inversely proportional to the square of the average transit time of blood cells through the sample volume. The remaining source is proportional to the Reynolds normal stress present at the measurement location [20]. The error in Reynolds normal stress measurements resulting from Doppler ambiguity has been previously quantified in measurements downstream of a stenosis [18]. These experiments showed that Reynolds normal stresses quantified by the ultrasound equipment used in these studies was 1.3 times greater than those quantified by hot wire anemometry. However, it was unknown whether average transit times of blood cells through the sample volume of this experiment were comparable. In addition, the effects of velocity gradient across the sample volume on velocity variance were unknown.

Another possible problem with these experiments is the use of the maximum velocity of the ultrasound transducer to quantify peak velocities and turbulent stresses. The use of the maximum velocity in this fashion is untested, and results from this method may depend heavily on the threshold used to distinguish signal from spectral noise.

To quantify possible error in Reynolds stress measurements resulting from transit time and velocity gradient effects and test whether the maximum velocity of the ultrasound transducer could be used to measure peak velocities, the equipment used in these studies was used to quantify mean velocity and velocity variance within a laminar, axisymmetric free jet. This jet had an orifice diameter similar to the width expected in a bileaflet valve leakage gap (0.2 mm), and its flow was set in motion by a 120 mm Hg water pressure head. The jet had an orifice velocity of 2.6 m/s in air, resulting in an orifice Reynolds number of approximately 520. The jet was submersed in water and oriented at an angle of 60 deg with respect to the ultrasound transducer used in these studies. To study this jet, the transducer was placed 25 diameters (5 mm) from the jet orifice. Common cornstarch, with particles of approximately 12 μm in diameter, was used to seed the flows. Mean and maximum velocity signals from the VingMed amplifier were obtained over 72 locations within the jet. At each location, these signals were sampled at a rate of 5 kHz by the analog/digital converter for 2 s. Ensemble averaging (Eq. (1)) of mean and maximum velocity measurements at each measurement location was used to determine velocity profiles. Eq. (3) was used to estimate the error introduced by transit time and velocity gradient effects at each measurement location.

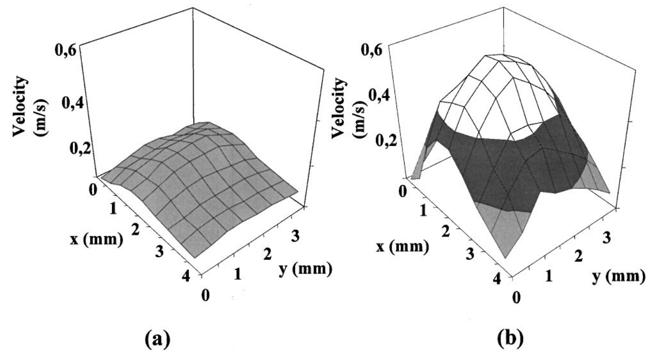

Fig. 4 Velocity profiles obtained from (a) mean velocity measurements and (b) maximum velocity measurements during the axisymmetric, laminar free jet experiment

Figure 4(a) and 4(b) show velocity profiles from mean and maximum velocity measurements in this experiment, respectively. An analytical estimate of the maximum jet velocity in the direction of the transducer (0.62 m/s) agreed very well with the peak velocity determined from maximum velocity measurements (0.60 m/s), and was similar in magnitude to the largest velocities measured in the in vivo experiment. This result shows that the maximum velocity of the ultrasound transducer is capable of reporting peak velocity in these experiments. The peak velocity determined from mean velocity measurements (0.18 m/s) was considerably less than those determined from either analytical estimation or maximum velocity measurements.

Velocity variance resulted in apparent Reynolds normal stresses of 2.0 N/m^2 using mean velocity measurements, and 1.9 N/m^2 using maximum velocity measurements. Since the jet studied was laminar, these apparent stresses account for errors due to spectral noise and transit time and velocity gradient effects. The following equation was therefore used to correct for errors caused by these phenomena:

$$\sigma_x=\left(\frac{\sigma_{x,PDU}-2}{1.3}\right) \tag{8}$$

Errors in turbulent stress estimation can also be introduced by the presence of coherent structures [21]. Since such structures are somewhat periodic in nature, their presence within a flow can be identified through examination of frequency spectra. The power spectrum of the fluctuating velocity component was therefore examined at each measurement location. Since no peaks were apparent in these spectra, periodic flow structures did not contribute to error in these measurements.

Ninety-five percent confidence intervals for the turbulent normal stress calculations were created from an estimator variance of a second-order moment [22], assuming a normal distribution of velocity measurements within each combination of phase window and measurement location.

Estimation of Maximum Turbulent Shear Stresses. Maximum turbulent shear stresses were analytically estimated from the calculated normal stresses. In deriving the analytical method, the turbulent kinetic energy equation:

$$U_j \frac{\partial}{\partial x_j}\left(\frac{1}{2}\overline{u_i u_i}\right) = -\frac{\partial}{\partial x_j}\left(\frac{\overline{u_j p}}{\rho} + \frac{1}{2}\overline{u_i u_i u_j} - 2\nu\overline{u_i s_{ij}}\right) - \overline{u_i u_j} S_{ij} - 2\nu\overline{s_{ij}s_{ij}} \tag{9}$$

was applied to the geometry of a leakage jet, assuming that the jet is axisymmetric, and that measurements were obtained near or before the position where the jet becomes fully developed. Taking the direction of the jet to be travelling along the 1 direction of a Cartesian coordinate system, these assumptions result in U_2, U_3, and $\partial/\partial x_1$ being very small and approximately equal to zero. It is then useful to analyze what each of the terms in Eq. (9) represent. The first terms on the right and left side of Eq. (9) represent turbulent kinetic energy transport by the mean flow, turbulent pressure fluctuations, turbulent velocity fluctuations, and viscosity. These terms will be grouped together and labeled T in the remainder of the analysis. The third term in Eq. (9) represents turbulent kinetic energy dissipation, and will be labeled ε in the remainder. The second term, which is the term of interest, represents the rate of production of turbulent kinetic energy. Using Cartesian coordinates to rewrite Eq. (9) in its three components, under the assumptions made:

$$1 \ \ \text{direction:} 0 = T - \frac{1}{2}\overline{u_1 u_2}\frac{\partial U_1}{\partial x_2} - \frac{1}{2}\overline{u_1 u_3}\frac{\partial U_1}{\partial x_3} - \varepsilon \tag{10}$$

$$2 \ \ \text{direction:} 0 = T - \frac{1}{2}\overline{u_1 u_2}\frac{\partial U_1}{\partial x_2} - \varepsilon \tag{11}$$

$$3 \ \ \text{direction:} 0 = T - \frac{1}{2}\overline{u_1 u_3}\frac{\partial U_1}{\partial x_3} - \varepsilon \tag{12}$$

Thus, the rate of production of turbulence in the 1-direction is equal to the sum of the rates of production in the 2 and 3 directions. This rate of production governs the amount of energy within the largest turbulent eddies in the jet. These eddies contain the majority of the energy in a turbulent flow, and the turbulent stress magnitudes are based on the energy contained within them. Since these eddies are located randomly within the flow field of the jet, and since the jet is axisymmetric, the spatial average of turbulent normal stress in the 1 direction is twice that of the stresses in the 2 and 3 directions:

$$\sigma_1 = 2\sigma_2 = 2\sigma_3 \tag{13}$$

Tennekes and Lumley [23] report that in addition to the axisymmetric jet geometry presented here, Eq. (13) is a good assumption in most pure two dimensional shear flows as well. The value of σ_1 can then be calculated from σ_x by rotating the coordinate system, using a method proposed by Grigioni et al. [24]. Since σ_1, σ_2, and σ_3 can be taken as the principal stress axes, no shear components of the turbulent stress tensor are needed to perform this rotation. Because σ_1 is the largest of the principal normal stresses, it is relabelled $\sigma_{\max}$:

$$\sigma_{\max} = \frac{\sigma_x}{\left(\cos^2\theta_x + \frac{1}{2}\cos^2\theta_y + \frac{1}{2}\cos^2\theta_z\right)} \tag{14}$$

θ_x, θ_y, and θ_z were defined as the angles between the x, y, and z axes defined in Fig. 3 and the axis of the jet. Values of these angles are documented in Table 1. If Eq. (14) holds, the maximum turbulent shear stress can be calculated directly from σ_x, as follows:

Table 1 Leakage jet correlation coefficients and angles with respect to coordinate system used

Jet	θ_x	θ_y	θ_z	α_{ana}
1	69°	57°	41°	0.44
2	74°	90°	16°	0.46
3	69°	57°	41°	0.44

$$\alpha_{ana} = \frac{1}{4\left(\cos^2\theta_x + \frac{1}{2}\cos^2\theta_y + \frac{1}{2}\cos^2\theta_z\right)} \tag{15}$$

These correlation factors are also reported in Table 1. A flow chart explaining the data analysis methods is shown in Fig. 5.

Results

Three turbulent stress maxima were observed within the interrogation area. Figure 6 shows the coordinates at which measurements were obtained within the interrogation area, and the assumed placement of the jets with respect to the St. Jude Medical valve. This figure also shows the spatial distribution of turbulent normal stress within each of the jets, determined by applying cyclic averaging in 20 ms time windows to maximum velocity data. From these plots, the location of the maxima and diameters of the leakage jets were determined (+/−1.5 mm and +/−1.0 mm, respectively). The maxima of jets 1 and 3 had the same y-coordinate, while the maximum of jet 2 was located 2.0 mm from the others in the y-direction. The location of the maxima of jet 2 was approximately equidistant from the maxima of jets 1 and 3. Jets 1 and 3 appeared circular in shape, with diameters of approximately 3 mm. The shape of the jets was difficult to determine, however, with the error associated with their diameter determination. The shape of jet 2 appeared to be more elliptical than circular in shape, with a small axis width of 2 mm and a large axis width of 2.5 mm.

Table 2 shows the peak velocity values obtained from each of these jets, both in the direction of the transducer and in estimated

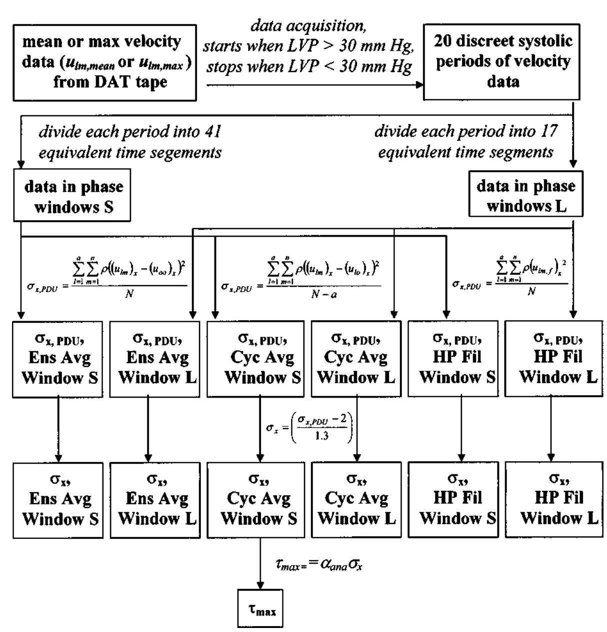

Fig. 5 Flow chart demonstrating data analysis method

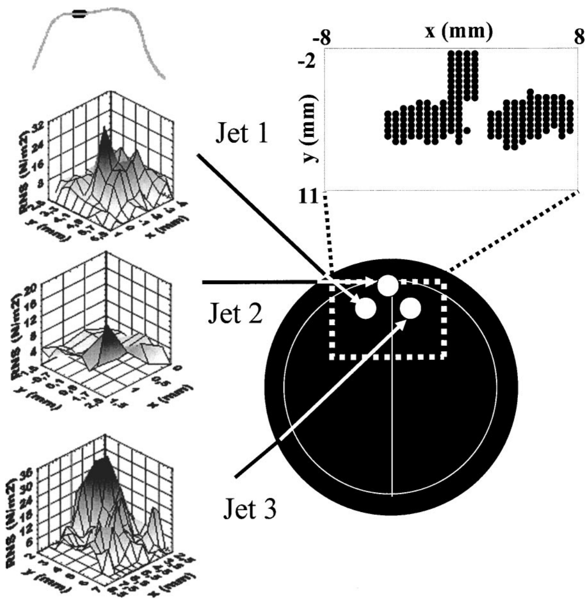

Fig. 6 Leakage jet locations within interrogation area, and with respect to the valve. Turbulent normal stresses during leakage flow, calculated from maximum velocity measurements, cyclic averaging, and 20 ms phase windows, are defined for each jet found. Dots on the 2-D plot above the valve show location within the interrogation area at which data were acquired.

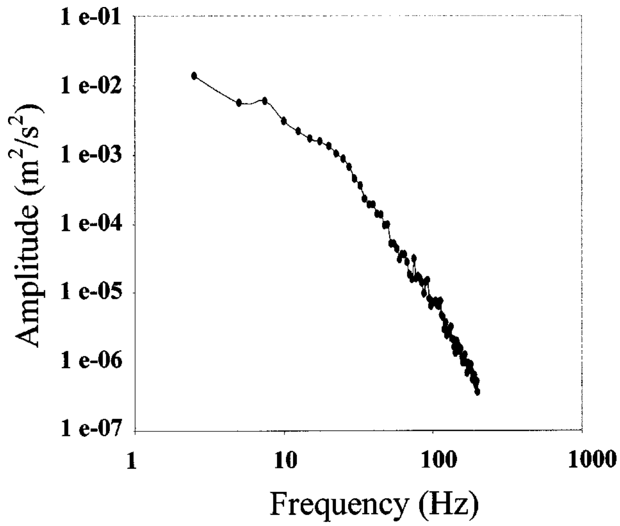

Fig. 7 Power spectrum of the measurements obtained from a specific location in jet 1

magnitude, using both phase windows. The uncorrected velocities of jets 1 and 3 were nearly the same (0.73 and 0.67 m/s, respectively, using phase window S), while jet 2 had a notably smaller velocity (0.39 m/s). Estimated peak velocity magnitudes were larger in jets 1 and 3 (2.04 and 1.87 m/s, respectively, using phase window S) than in jet 2 (1.41 m/s). Decreasing the phase window size resulted in an average increase of 4% in the peak velocity calculated from each of the jets. Based on these velocity measurements, the approximate width of the jets (0.5 mm for jet 2), and a kinematic viscosity of 3.0 cSt, the Reynolds numbers of jets 1 and 3 were estimated at 2100, while the Reynolds number of jet 2 was approximately 800.

Figure 7 shows the power spectrum of the fluctuating component of the maximum velocity signal at the location where the highest turbulent stress was observed in this experiment. There are no notable peaks in the spectrum, and there appear to be two slopes. One of these has a value of approximately 1.2 and encompasses frequencies from 10 to 30 Hz. The other has a value of approximately 4.2 encompasses frequencies from 30 to 200 Hz. The power spectra of the fluctuating components of velocity at other measurement locations displayed similar behavior. No notable peaks were found in any of these spectra. In many, there was no clear distinction between slopes, but in all the slope was increasing at 30 Hz, and in most the slope of the section between 10 and 20 Hz was between 1.0 and 1.6 and the slope of the section between 150 and 200 Hz was between 4 and 5.

The highest turbulent normal stress values calculated from each of the jets, using mean velocity measurements and maximum velocity measurements, are shown in Tables 3 and 4, respectively. The magnitude of turbulent normal stress estimates depended heavily on the data and analysis technique used. The velocity data used to calculate these estimates (mean or maximum) had the

Table 2 95% confidence intervals of maximum velocities measured within leakage jets, and predicted peak axial velocities of jets

	$(u_{oo})_x$ (m/s)		u_{peak} (m/s)	
Jet	Window S	Window L	Window S	Window L
1	0.73 ± 0.03	0.72 ± 0.01	2.04	2.01
2	0.39 ± 0.01	0.36 ± 0.01	1.41	1.31
3	0.67 ± 0.01	0.65 ± 0.01	1.87	1.81

Table 3 95% confidence intervals of highest turbulent normal stress magnitudes calculated from mean velocity measurements

	σ_x (N/m^2)					
Jet	Ens Avg Window S	Ens Avg Window L	Cyc Avg Window S	Cyc Avg Window L	HP Fil Window S	HP Fil Window L
1	8 ± 1	9 ± 1	2 ± 0	5 ± 0	7 ± 1	8 ± 1
2	8 ± 1	6 ± 0	2 ± 0	3 ± 0	5 ± 1	4 ± 0
3	14 ± 1	12 ± 1	3 ± 0	4 ± 0	8 ± 1	6 ± 0

Table 4 95% confidence intervals of highest turbulent normal stress magnitudes calculated from maximum velocity measurements

	σ_x (N/m^2)					
Jet	Ens Avg Window S	Ens Avg Window L	Cyc Avg Window S	Cyc Avg Window L	HP Fil Window S	HP Fil Window L
1	294 ± 26	268 ± 15	46 ± 4	112 ± 6	69 ± 6	55 ± 3
2	132 ± 12	108 ± 6	15 ± 1	48 ± 3	40 ± 4	28 ± 2
3	168 ± 15	151 ± 8	25 ± 2	53 ± 3	47 ± 4	35 ± 2

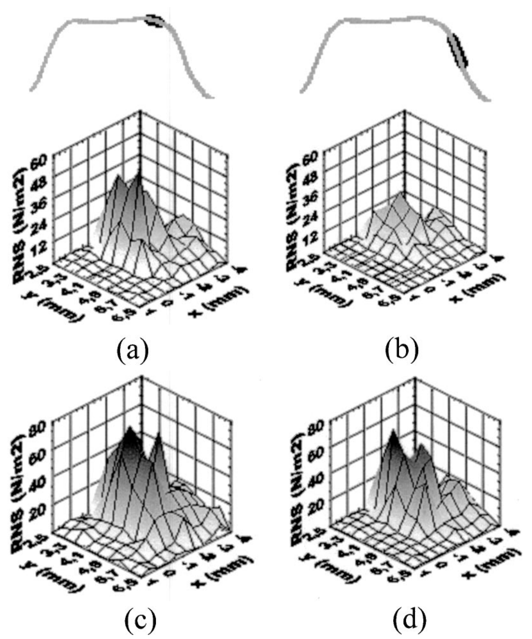

Fig. 8 Phase delay introduced by high pass filtering. (a) and (b) were created from data which were cyclic averaged, while (c) and (d) were created from data which were high pass filtered. The phase windows over which analyses were completed are shown in the left ventricular pressure curves above (a) and (b).

largest effect on their magnitudes. The highest estimates of the turbulent normal stress calculated from mean velocity measurements obtained in jets 1, 2, and 3 were 9 N/m^2, 8 N/m^2, and 14 N/m^2, respectively. The highest turbulent normal stress estimates calculated from maximum velocity measurements obtained in jets 1, 2, and 3 were 294 N/m^2, 132 N/m^2, and 168 N/m^2. Analysis technique had a notable effect on estimates of turbulent normal stress as well. Estimates of peak turbulent normal stress magnitude by ensemble averaging were an average of 406% higher than estimations made by cyclic averaging and 277% higher than estimates made by high pass filtering. Estimates made by cyclic averaging and high pass filtering were comparable, particularly if these estimates were made from mean velocity measurements. To a lesser extent, estimates dependent on the size of the phase window used in the analysis. Estimates made by ensemble averaging and high pass filtering increased as phase window size decreased, while estimations made by cyclic averaging decreased with phase window size.

Figure 8 shows spatial plots of the turbulent normal stresses in jet 1 during the later part of systole. These stresses were calculated from maximum velocity measurements using phase window S. The spatial plots of Figs. 8(*a*, *b*) were constructed from data analyzed by cyclic averaging, while the spatial plots in Figs. 8(*c*, *d*) were constructed from data analyzed by high pass filtering. The curves above the plots represent the systolic portion of the left ventricular pressure waveform, and the shaded portion of each curve represents the cyclic timing of the phase window over which data in each plot were analyzed. As the left ventricular pressure began to decrease, turbulent normal stresses calculated by cyclic averaging decreased immediately. With the high pass filtering technique, however, a time delay was present between the decrease in left ventricular pressure and the decay in magnitude of the turbulent normal stresses.

Discussion

General. The leakage pattern observed in these experiments has been reported by a number of observers in vitro [9,11,25]. In these experiments, it was seen that one jet emerges from each of the four pivots, and two additional jets are formed at the locations where the intersection of the two leaflets meets the valve housing. From these experiments, it can be reasonably assumed that jets 1 and 3 originated from the pivots, while jet 2 originated from a location where the intersection of the leaflets met the valve housing.

The estimated velocity magnitudes are somewhat higher than velocity estimates observed in previous in vitro laser Doppler velocimetry investigations of the St. Jude Medical valve [9,11,12]. These works reported maximum leakage velocities between 0.7 and 1.0 m/s. Steegers et al. [9] used the same valve and flow conditions for a series of pulsed Doppler ultrasound and laser Doppler velocimetry experiments. These researchers found a notably higher maximum velocity (1.25 m/s) with Doppler ultrasound than they saw in their laser Doppler velocimetry experiments. The differences observed in leakage velocity could originate from the tendency of angle corrected measurements to overestimate the jet centreline velocity magnitude, as discussed by Yoganathan et al. [26]. They could also originate from the analysis technique used to make the measurements. Because the diameter of leakage jets, reported as approximately 1.0 mm [9,11], is on the same order of magnitude as the sample volume diameter of a laser Doppler velocimeter, there will be significant velocity gradients across the sample volume when the sample volume is positioned at the jet centerline. Averaging of these measurements will thus result in a velocity somewhat smaller than the centerline velocity. Velocity determination by pulsed Doppler ultrasound, on the other hand, is not necessarily limited by the size of the sample volume interrogated by the transducer. In this study, the number of reflecting particles (the cells of the blood) within the sample volume at any given time was on the order of 10^7. Because the concentration of blood cells within the sample volume was very large, the transducer received a spectrum of frequencies during its sampling time. The ultrasound transducer has the option of using the maximum (or minimum) of this band of frequencies to compute velocity. These frequencies correspond to a small group of blood cells that are moving within the center of the leakage jet. Thus, pulsed Doppler ultrasound can perhaps give a higher and more accurate measure of the maximum leakage jet velocity than laser Doppler velocimetry. Differences in velocity measured in these experiments and in vitro could also result from geometrical differences between in vitro heart simulators and the in vivo environment. The atrial chamber of the pig had a volume of approximately 20 mL, considerably smaller than the atrial chamber used in many in vitro simulators. Incoming atrial forward flow, which occurs at the same time as mitral valve leakage, enters the atrium in a direction nearly parallel to the plane of the valve, and could alter both the velocity and direction of the leakage jets.

The power spectra of the measurements had shapes characteristic of nondeterministic signals, with no notable peaks and a gradually increasing negative slope. Thus, contamination of the turbulent stress calculations from coherent structures was negligible, and a means of separating these components was deemed unnecessary. The slopes of the spectra cannot be taken to represent the smaller scales of the turbulent flow, as the frequency response of the Doppler instrument was not sufficient to allow the measurement of these scales.

Comparison of Data and Analysis Techniques. The choice of velocity data type had a large effect on the magnitudes of turbulent normal stresses. This could be expected, as the width of the ultrasound sample volume is of the same order of magnitude as the width of the leakage jets studied. Previous experiments [9] have estimated the widths of leakage jets of a St. Jude Medical size 27 valve 1 mm proximal to the pivot guards at between 0.8 and 1.2 mm. The widths of the leakage jets in this study were estimated between 0.5 and 3.0 mm. Thus, during at least some of the locations at which measurements were obtained, and quite possibly all of them, the sample volume was not completely contained within the jet structure. The use of mean velocity over the sample volume to calculate turbulent stress therefore introduces error into the calculations. This error is associated with the fact that a considerable portion of the sample volume is located outside the turbulent portion of the jet. Because of this, turbulent fluctuations measured by the transducer will be dampened by averaging with the velocity measurements obtained within the portion of the sample volume outside the jet, and the turbulent stress calculated by mean velocity measurements will be lower than the actual turbulent stress within the jet.

The use of maximum velocity within the sample volume to calculate turbulent stress may be a better solution. Since large scale fluctuations in maximum velocity within the sample volume are caused by large scale eddies, the maximum velocity can measure the movement of the largest turbulent eddies within a flow. Since all turbulent energy originates in these larger eddies, the maximum velocity function can be used to measure turbulent stress. A potential problem with the use of this function is that the maximum velocity in these experiments was measured independently of whether it was moving toward or away from the transducer. Because of this, abrupt changes in velocity measurement could be caused by small changes in jet direction, which may not necessarily be due to turbulent eddies. Thus, the turbulent stress calculated from maximum velocity measurements will be higher than the actual turbulent stress within the jet.

A potential problem with the ultrasound technique in general remains in determining exactly where the largest stress is located. Whether the location of this large magnitude stress lies in the center or the edge of the sample volume, the mean or maximum output from the transducer will be nearly the same. If a spatial map of turbulent stress is made from these measurements, the jet may appear to be twice the sample volume size wider than it truly is. This may explain why the diameters of jets 1 and 3 (3.0 mm) were so large compared to the jet widths observed by laser Doppler velocimetry. If this is true, the Reynolds numbers calculated in this analysis are up to a factor of three lower than reported. Flow begins to transition to turbulence at orifice Reynolds numbers of approximately 30 for 2-D, planar jets and Reynolds numbers of 1000 for circular jets [27]. Reynolds numbers of approximately 3000 are required for fully developed turbulent flow [27]. Thus, jets 1 and 3 were likely in the middle of the transitional regime. Jet 2 was near the beginning of the transitional regime, and more stable in nature than jets 1 and 3. This analysis is supported by the magnitudes of the turbulent normal stresses calculated from mean and maximum velocity measurements. In nearly all of the analysis techniques used, the turbulent normal stresses found in jet 2 were smaller than those in jets 1 and 3.

The choice of analysis technique also had a large effect on the calculated turbulent stresses. Cyclic variation was observed to have much more of an effect on turbulence calculations in vivo than in previous in vitro experiments [11]. This may be because the atrial wall was located very close to the valve in this experiment, and its position may change from cycle to cycle. It may also be caused by cyclic changes in incoming atrial flow. Some means of removal of cyclic variation is necessary in these in vivo experiments. This can be accomplished either by cyclic averaging or high pass filtering. The use of the high pass filtering technique, however, creates a phase delay in the velocity measurements with respect to cycle time. This was observed in the form of a delay in the fall of turbulent stress with left ventricular pressure in the spatial maps of Fig. 8. The phase delay imposed by the Butterworth filter used in these studies is nonuniform, and could be a reason why magnitudes of turbulent stress rose with decreasing phase window size. The high pass filter could be optimized to minimize or completely eliminate phase shift. It should be noted, however, that any high pass filter introduces either slight phase shift or alters the amplitude of the velocity signal. Thus, of the three techniques investigated, cyclic averaging was thought to be the most effective for these studies.

Table 5 Maximum turbulent shear stress magnitudes estimated from mean and maximum velocity measurements

Jet	$\tau_{\max}$ (N/m^2)	
	$u_{ij(\text{mean})}$	$u_{ij(\max)}$
1	1	20
2	1	7
3	1	12

Phase window width was found to have a significant effect on turbulent normal stresses calculated from maximum velocity measurements, though the magnitude of this effect was less than either data type or data analysis method. It is well known that decreasing phase window width increases temporal resolution of the turbulence measurements, while decreasing the statistical accuracy of the calculated turbulent stress. A previous steady flow study of leakage jets [11] has shown that in phase windows of 20 ms, sample sizes of at least 500 measurements are necessary for statistical accuracy in calculations of turbulent stress. Since both phase window sizes contained a minimum of 1700 measurements, the statistical accuracy of the calculations in each phase window should be sufficient. The 95% confidence intervals in Tables 4 and 5 support this assessment. The majority of the differences in the magnitudes of turbulent stress were therefore caused by changes in temporal resolution. If either the speed or the direction of the jets changes over time, a large time window can artificially inflate calculations of turbulent stress [28]. A change in the speed of the jets could be brought about by a change in the pressure difference on each side of the valve during the systolic phase. Left ventricular pressure remained approximately constant over systole, but the left atrial pressure rose approximately 20 mm Hg during this period. This rise corresponded temporally with a decrease in mean velocity (Fig. 9). Because the smallest time windows studied were approximately 20 ms, they were thought to be most appropriate for reporting turbulent stresses.

The use of the analytical correlation coefficients to report maximum turbulent shear stresses affects the magnitudes of the calculated stresses, and there are possible problems with the use of these coefficients. Calculations using the analytical coefficients assume an axisymmetric jet. Jets emitted from asymmetric and slit-like orifices become more axisymmetric in their velocity profile during their downstream development [29], but how assymmetry affects the turbulence characteristics of the jets is unknown. However, since Tennekes and Lumley [23] report that Eq. (13) holds for most pure two-dimensional shear flows, turbulent stress magnitudes may not depend heavily on jet shape.

Comparison of TSS Magnitudes with Laser Doppler Velocimetry Studies. Ellis et al. performed the first comprehensive experimental quantification of leakage emitted from the pivots of the SJM design [7]. They studied the leakage flow 1 mm proximal to one pivot guard of a SJM Standard size 27 aortic valve using three component laser Doppler velocimetry. Turbulent shear stresses in the experiments of Elles et al. were determined by ensemble averaging over 20 ms time windows. The mean aortic pressure during diastole in these experiments was 120 mm Hg, and the largest turbulent shear stress reported during the middle of diastole was 80 N/m^2. Steegers et al. performed a similar study on all four pivots of a SJM mitral valve, at a number of axial distances from the valve [9]. Claiming that laser Doppler velocimetry could not adequately resolve the small scales of turbulent flow, these researchers used an empirical method to calculate turbulent shear stresses from the velocity gradient of the jet. The peak ventricular pressure measured in these experiments was 130 mm Hg, and the largest turbulent shear stress reported in the leakage flow was 50 N/m^2. Travis et al. studied leakage from a SJM Regent size 17 valve 1 mm proximal to the pivot guards under aortic conditions [11]. These researchers used ensemble and cyclic av-

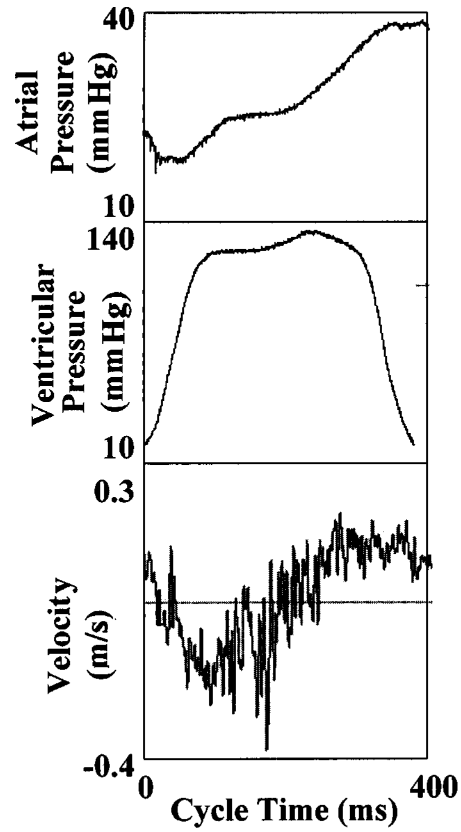

Fig. 9 Left atrial pressure, left ventricular pressure, and velocity over systole. The rise in left atrial pressure corresponds with a decrease in velocity.

eraging to calculate turbulent shear stresses obtained under an aortic pressure head of 120 mm Hg. They reported a maximum turbulent shear stresses of 29 N/m^2, using ensemble averaging, and 27 N/m^2, using cyclic averaging over 20 ms phase windows. Most recently, Meyer et al. studied the turbulent shear stresses resulting from leakage of a SJM mitral valve driven by a ventricular pressure of 120 mm Hg [16]. After ensemble averaging in 1 ms phase windows, these researchers reported a maximum turbulent shear stress of 45 N/m^2. Maxima in turbulent shear stress within the leakage 1 mm upstream of the SJM pivot guards have thus been reported between 27 and 80 N/m^2.

To accurately compare the results in this work with previous studies, appropriate analysis techniques must be identified and implemented on the data in this study. Most previous laser Doppler velocimetry studies of leakage jets [7,11,16] have used ensemble averaging in the analysis. One of these has shown that cyclic variations have little effect on turbulent stresses calculated in vitro [11]. Cyclic variations contaminated calculations of the turbulent stresses to a large extent in this study. Together, these observations suggest that results obtained from ensemble averaging in previous in vitro studies should be more similar to those obtained from cyclic averaging than those obtained from ensemble averaging in this study. Cyclic averaging was therefore chosen as the analysis technique for comparison between this and previous studies. The studies that reported the two extremes in the reported range of turbulent shear stress magnitudes [7,11] used 20 ms phase windows in their analysis. This approximate size of time window was therefore applied to the data of this study for comparison. The resulting turbulent normal stresses were multiplied by the analytical correlation coefficient to determine maximum turbulent shear stress magnitudes. The largest shear magnitudes calculated using these analysis techniques were 1 and 20 N/m^2 for mean and maximum velocity measurements, respectively. Thus, maximum turbulent shear stresses estimated from mean velocity measurements in this study are over an order of magnitude less than those measured in previous studies, and maximum turbulent shear stresses estimated from maximum velocity measurements are slightly lower than the range reported in previous studies.

Conclusions

This study introduced an in vivo method of measuring turbulence in the leakage jets of a prosthetic heart valve, using pulsed Doppler ultrasound. The study focused on the development of appropriate data analysis techniques for this method. The technique chosen applies cyclic averaging to mean and maximum velocity measurements within small, normalized phase windows to calculate Reynolds normal stresses in the direction of the ultrasound beam. The importance of the removal of cyclic variation in velocity measurements and the use of small phase windows in the analysis of velocity data from leakage jets was shown. An analytical technique relating one dimensional velocity measurements to maximum turbulent shear stress for shear flow was introduced and applied to the data from these experiments. The stresses observed were smaller than those reported from previous in vitro simulations.

Acknowledgments

The authors wish to thank Tanya Thomsen and the perfusionists from the Department of Cardiothoracic and Vascular Surgery for their time and expertise in performing this experiment, and St. Jude Medical for their donation of valve used in this study. The authors also wish to recognize the International Research Fellowship Program of the U.S. National Science Foundation (Grant INT 0107348) for their generous financial support.

List of Symbols

a	number of cycles (dimensionless)
N	number of measurements (dimensionless)
n	number of measurements in cycle l (dimensionless)
p	fluctuating pressure (N/m^2)
S_{ij}	time-averaged strain rate acting in the i direction on a plane normal to direction j (1/s)
s_{ij}	fluctuating strain rate acting in the i direction on a plane normal to direction j (1/s)
T	turbulent energy transport rate per unit mass (m^2/s^3)
U_j	time-averaged velocity in direction j (m/s)
u_i, u_j	fluctuating velocity in directions i and j (m/s)
u_{lm}	single velocity measurement from cycle l (m/s)
u_{lmf}	high pass filtered velocity measurement from cycle l (m/s)
u_{lo}	average velocity of measurements in cycle l (m/s)
u_{peak}	jet centerline velocity (m/s)
u_{oo}	average velocity of all measurements (m/s)
u_1, u_2, u_3	fluctuating velocity along principal stress axes 1, 2, and 3 (m/s)
α_{ana}	analytical correlation coefficient between σ_x and $\tau_{\max}$ (dimensionless)
ε	turbulent energy dissipation rate per unit mass (m^2/s^3)
ν	kinematic viscosity (m^2/s)
$\theta_x, \theta_y, \theta_z,$	angle between Cartesian coordinate axes (defined in Fig. 3) and jet axis (radians)
ρ	density (kg/m^3)
$\sigma_{x,PDU}$	turbulent normal stress measured by ultrasound (N/m^2)
σ_x	turbulent normal stress along direction of measurement (N/m^2)
$\sigma_1, \sigma_2, \sigma_3$	turbulent normal stress along principal stress axes (N/m^2)

σ_{max} maximum turbulent normal stress (N/m^2)
τ_{max} maximum turbulent shear stress (N/m^2)

References

[1] Hasenkam, J. M. et al., 1996, ''Hemodynamic evaluation of a new bileaflet valve prosthesis: an acute animal experimental study,'' J. Heart Valve Dis., **5**(6), pp. 574–580.
[2] Yoganathan, A. P., personal communication.
[3] Gross, J. M. et al., 1996, ''A microstructural flow analysis within a bileaflet mechanical heart valve hinge,'' J. Heart Valve Dis., **5**(6), pp. 581–590.
[4] Ellis, J. T. et al., 1996, ''Velocity measurements and flow patterns within the hinge region of a Medtronic Parallel bileaflet mechanical valve with clear housing,'' J. Heart Valve Dis., **5**(6), pp. 591–599.
[5] Woo, Y. R., and Yoganathan, A. P., 1986, ''In vitro pulsatile flow velocity and shear stress measurements in the vicinity of mechanical mitral heart valve prostheses,'' J. Biomech., **19**(1), pp. 39–51.
[6] Baldwin, J. T. et al., 1991, ''Mean velocities and Reynolds stresses within regurgitant jets produced by tilting disc valves,'' ASAIO Trans., **37**(3), pp. M348–M349.
[7] Ellis, J. T. et al., 1996, ''An in vitro investigation of the retrograde flow fields of two bileaflet mechanical heart valves,'' J. Heart Valve Dis., **5**(6), pp. 600–606.
[8] Maymir, J. C. et al., 1997, ''Effects of tilting disk heart valve gap width on regurgitant flow through an artificial heart mitral valve,'' Artif. Organs, **21**(9), pp. 1014–1025.
[9] Steegers, A. et al., 1999, ''Leakage flow at mechanical heart valve prostheses: improved washout or increased blood damage?,'' J. Heart Valve Dis., **8**(3), pp. 312–323.
[10] Ellis, J. T., and Yoganathan, A. P., 2000, ''A comparison of the hinge and near-hinge flow fields of the St Jude medical hemodynamic plus and regent bileaflet mechanical heart valves,'' J. Thorac. Cardiovasc. Surg., **119**(1), pp. 83–93.
[11] Travis, B. R. et al., 2002, ''An analysis of turbulent shear stresses in leakage flow through a bileaflet mechanical prostheses,'' J. Biomech. Eng., **124**(2), pp. 155–165.
[12] Meyer, R. S. et al., 2001, ''Laser Doppler velocimetry and flow visualization studies in the regurgitant leakage flow region of three mechanical mitral valves,'' Artif. Organs, **25**(4), pp. 292–299.
[13] Lamson, T. C. et al., 1993, ''Relative blood damage in the three phases of a prosthetic heart valve flow cycle,'' ASAIO Trans., **39**(3), pp. M626–M633.
[14] Travis, B. R. et al., 2001, ''Bileaflet aortic valve prosthesis pivot geometry influences platelet secretion and anionic phospholipid exposure,'' Ann. Biomed. Eng., **29**(8), pp. 657–664.
[15] Travis, B. R. et al., 2001, ''The sensitivity of indicators of thrombosis initiation to a bileaflet prosthesis leakage stimulus,'' J. Heart Valve Dis., **10**(2), pp. 228–238.
[16] Cockelet G., ''The rheology of human blood'' Fung Y.
[17] Pohl, M. et al., 1996, ''In vitro testing of artificial heart valves: comparison between Newtonian and non-Newtonian fluids,'' Artif. Organs, **20**(1), pp. 37–46.
[18] Nygaard, H. et al., 1994, ''A new perivascular multi-element pulsed Doppler ultrasound system for in vivo studies of velocity fields and turbulent stresses in large vessels,'' Med. Biol. Eng. Comput., **32**(1), pp. 55–62.
[19] Nygaard, H. et al., 1994, ''Turbulent stresses downstream of three mechanical aortic valve prostheses in human beings,'' J. Thorac. Cardiovasc. Surg., **107**(2), pp. 438–446.
[20] Garbani, J. L., Forster, F. K., and Jorgensen, J. E., 1982, ''Measurement of fluid turbulence based on pulsed ultrasound techniques,'' J. Fluid Mech., **118**, pp. 445–470.
[21] Lieber, B. B. et al., 1989, ''On the discrimination between band-limited coherent and random apparent stresses in transitional pulsatile flow,'' J. Biomech. Eng., **111**(1), pp. 42–46.
[22] Benedict, L. H., and Gould, R. D., 1996, ''Towards better uncertainty estimates for turbulent statistics,'' Exp. Fluids, **22**, pp. 129–136.
[23] Tennekes, H., and Lumley, J. L. 1972, A first course in turbulence MIT Press, Cambridge, Mass.
[24] Grigioni, M. et al., 2000, ''On the monodimensional approach to the estimation of the highest reynolds shear stress in a turbulent flow,'' J. Biomech., **33**(6), pp. 701–708.
[25] Flachskampf, F. A. et al., 1991, ''Patterns of normal transvalvular regurgitation in mechanical valve prostheses,'' J. Am. Coll. Cardiol., **18**(6), pp. 1493–1498.
[26] Yoganathan, A. P. et al., ''Oblique flow vectors from dispersing jets produce the velocity overestimation on angle corrected continuous wave Doppler studies: in vitro laser Doppler investigations,'' Circulation, **76**(Supp IV), pp. 355.
[27] Blevins, R. D. 1984, Applied fluid dynamics handbook Van Nostrand Reinhold Co., New York, N.Y.
[28] Sahn, D. J., 1988, ''Instrumentation and physical factors related to visualization of stenotic and regurgitant jets by Doppler color flow mapping,'' J. Am. Coll. Cardiol., **12**(5), pp. 1354–1365.
[29] Stewart, S. F., Burte, F., and Clark, R. E., 1993, ''Quantification of asymmetric valvular regurgitant jets by color Doppler ultrasound in vitro,'' Echocardiography, **10**(1), pp. 23–36.